



A rock magnetic profile through the ejecta flap of the Lockne impact crater (central Sweden) and implications for the impact excavation process



Irene Melero-Asensio^{a,*}, Fátima Martín-Hernández^{b,c}, Jens Ormö^a

^a Centro de Astrobiología (INTA-CSIC), Carretera de Ajalvir km 4, Torrejón de Ardoz, Madrid 28850, Spain

^b Department of Geophysics, Faculty of Physics, Universidad Complutense de Madrid, Madrid 28040, Spain

^c Instituto de Geociencias (UCM-CSIC), Faculty of Physics, Madrid 28040, Spain

ARTICLE INFO

Article history:

Received 11 March 2014

Accepted 7 November 2014

Available online 18 November 2014

Keywords:

Impact crater

Rock magnetism

Marine target

Flap formation process

Lockne crater

ABSTRACT

The well-documented, well-preserved, and well-exposed Lockne crater is a reference crater for marine-target impacts on Earth. The large amount of data allows detailed analysis of the cratering and modification processes. A unique feature of Lockne as compared with other similar craters is its pristine ejecta layer. Here, we provide the first complete lithological description coupled with an analysis of the rock magnetic properties of the Lockne-9 core drilled through the ejecta flap. Low-field bulk magnetic susceptibility, magnetic hysteresis, isothermal remanent magnetization curves (IRM), and the corresponding model of the coercivity spectra, backfield IRM, and thermomagnetic curves are used to fully characterize the magnetic mineralogy (i.e., pseudo-single domain (PSD) magnetite and pyrite). Variation of the magnetic properties with depth reveals a characteristic maximum in the magnetic susceptibility and magnetization within the crystalline ejecta. The magnetic properties of rocks affected by the impact show a slight weakening in the coercivity of magnetic minerals in comparison with rocks not affected by the impact. Altogether, this suggests to us that the high magnetization zone already existed before the impact event took place. Therefore, it can be inferred that during the cratering process, the Lockne ejecta was repositioned *en masse* from the central part of the crater in the form of an ejecta flap. This stands in contrast to the standard ballistic emplacement model wherein individual particles move in an ejecta curtain.

© 2014 Elsevier B.V. All rights reserved.

1. Introduction

The 458 million years old Lockne crater in central Sweden (Fig. 1) is today one of the best accessible, well-preserved marine-target craters on Earth because of the fact that—immediately after its formation—the crater was covered by post-impact marine sediments and, subsequently, by over-thrusted Caledonian nappes (Lindström et al., 2005a). It was thus protected from erosion until Cenozoic isostatic uplift and Pleistocene glaciations event exposed the crater. This fortunate set of circumstances has triggered many geological and geophysical studies during the last few decades, spanning the pre-impact sedimentary record, impact process, and post-impact sedimentation (e.g., Sturkell, 1998; Lindström et al., 2005a; Ormö et al., 2010b; Sturkell et al., 2013, and references therein). This impact structure has been explored by 11 short core drillings (Fig. 1), and over 5000 outcrop descriptions, which is the basis for a detailed geological map (i.e., Lindström et al., 2005a). In addition, this impact crater has been the site of several geophysical surveys (e.g., Sturkell and Ormö, 1998; Sturkell et al., 1998b). Cores 1–6 were drilled in order to constrain the crater dimensions and to determine

the stratigraphy of the crater infill and the biostratigraphic age of the crater (Lindström et al., 1996). Drill cores 7, 8, and 9 (the latter being the subject of this study) were obtained during 2004 with the main objective to study the depositional environment within the crater as well as the ejecta dynamics (Ormö and Lindström, 2005). A brief description of the Lockne-9 core is given by Ormö and Lindström (2005), and a study on biomineralization at certain core levels was carried out by Lindgren et al. (2007). Drill cores 10 and 11 are subject for an ongoing geological and geophysical study (Sturkell et al., work in progress). Previous geophysical studies include modeling of the gravimetric and magnetic anomalies generated by the crater (Sturkell and Ormö, 1998; Sturkell et al., 1998b). The magnetic modelling was restricted to the use of aeromagnetic anomalies and measured values of the induced magnetization (i.e., magnetic susceptibility) for the geological bodies in consideration. The magnetic signature of the crater is very weak due to the low contrast between the main lithologies (Sturkell and Ormö, 1998) and for simplicity, remanent magnetization as a contribution to the total signal was not considered.

Rock magnetism and paleomagnetism analysis related with impact cratering are commonly used for two main purposes: magnetic modelling and studies of shock effects. Rock magnetic characterization allows the magnetic susceptibility as initial input in the modelling of magnetic

* Corresponding author. Tel.: +34 915872982.

E-mail address: meleroi@cab.inta-csic.es (I. Melero-Asensio).

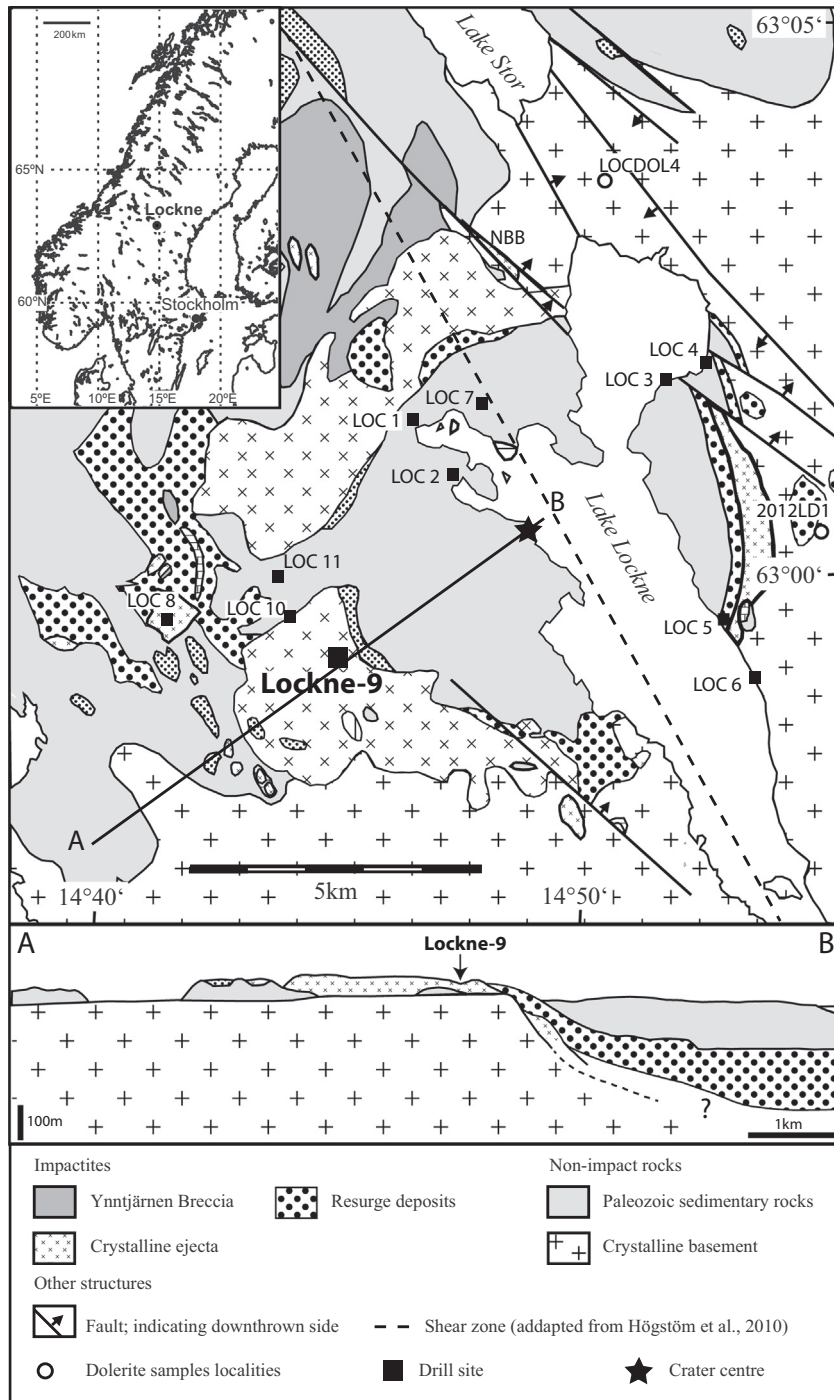


Fig. 1. Geological map and location of Lockne-9 drill core with respect to the crater centre (modified from Lindström et al., 2005a and Frisk and Ormö, 2007). The lower panel displays a simplified geological section through the Lockne crater passing by the Lockne-9 core (modified from Lindström et al., 2005a).

anomalies (e.g., Henkel and Reimold, 2002; Henkel et al., 2002; Ormö et al., 2010a; Scott et al., 1997). Paleomagnetic studies constrain the amount of remanent magnetization that contributes to the magnetic anomaly model (e.g., Elbra et al., 2009). Combined analysis in pyrrhotite-bearing rocks has been applied to understand shock demagnetization by impacts on Earth and other planetary bodies (e.g., Kontny et al., 2007; Louzada et al., 2010).

1.1. Setting of the Lockne-9 drilling

The formation of the Lockne crater in an epicontinental sea of about 500 m water depth is of interest as the layer of seawater is known to affect

the excavation process and the ejecta emplacement (e.g., Lindström et al., 2005b; Ormö and Lindström, 2000; Shuvalov et al., 2005). So far, there is not much known about the ejection process at marine impacts with such a relatively deep target water depth as Lockne (i.e., a water depth equal or more than the projectile diameter). Especially enigmatic is the apparent absence of a structural uplift (Fig. 1) below the ejecta of the rim area (e.g., Sturkell and Lindström, 2004), which is common at the land-target craters more frequently used as standards for crater morphologies (e.g., Melosh, 1989 and references therein). Instead, the formation of exceptionally wide, relatively coherent ejecta flaps is realized in this setting (e.g., Lindström et al., 2005a). It is possible that these features are a consequence of the low position of the basement crater below a

target succession of sedimentary cover rocks and seawater. The upper and weaker and less dense part of the target is subject to a shallow excavation flow generating a concentric growth of the transient crater with a lower, nested part of the crater formed in the basement (e.g., Gault and Sonett, 1982; Shuvalov and Trubetskaya, 2008). The nested basement crater is the source for the crystalline ejecta flaps that covers parts of the floor of the surrounding, outer crater (Lindström et al., 2005a). A cross section through the northern part of the Lockne ejecta flap is exposed in the Nordanbergsberget quarry (labeled as NBB in Fig. 1). The overturned flap is here resting on remnants of the Cambrian sedimentary target succession that have been sandwiched between a nearly horizontal sub-Cambrian peneplain and the ejecta masses (Lindström et al., 1996). The thickness of the ejecta flap is at this location approximately 10–15 m but has been estimated to be about 20–30 m in more proximal locations along the western crater rim (Sturkell and Lindström, 2004). Numerical modeling by Lindström et al. (2005b) describes Lockne as formed by an oblique impact (45° from the East), which caused a better developed flap on the down-range, western, side of the structure. On the eastern side, the crystalline ejecta is only a few meters thick and covers a much narrower area outside the rim. This is considered a primary feature as the ejecta are in places covered by early modification stage resurge deposits (Lindström et al., 2005a).

The concentric morphology of the Lockne crater is expressed in its 7.5 km wide, deeper, inner crater developed in the crystalline basement, and the surrounding 3.5 km wide brim where the crater excavation removed most of the 80 m sedimentary cover rocks (mainly 50 m of limestone covering 30 m of dark mud, i.e., today's alum shale) and the 500 m of seawater. The brim was partially covered by the crystalline ejecta flap from the basement crater shortly before the initiation of the water resurge toward the inner crater (Lindström et al., 2005a). The result is a soup-plate-like crater with a smaller, nested crater surrounded by a wider (approximately 14 km in diameter) outer crater. The crystalline rocks of the basement are mainly Proterozoic granitoids, within metavolcanites, which are exposed at the southern part of the crater (Lindström and Sturkell, 1992; Lindström et al., 1996; Sturkell, 1998a). The basement rocks also include dolerite sills, which are several tens of meters thick and hundreds of meters wide (Patchett, 1978). Other geological features of the crater and its surroundings of interest to this study include crystalline breccias and hydrothermal altered rocks. Crystalline breccias can be found within the nested, basement crater and as part of the ejecta layer surrounding it. Hydrothermal alteration of rock has in the area occurred both before (e.g., major shear zones), during (i.e., impact heated rock), and after (e.g., Caledonian orogeny) the impact.

The unique setting of the Lockne crater makes it a reference example of concentric craters in layered targets (e.g., Högström et al., 2010; Ormö et al., 2013). Therefore, it has been proposed as a high priority target, together with the Siljan crater (the largest impact crater of Western Europe), for the Swedish Deep Drilling Program (SDDP).

In order to investigate the mode of ejecta emplacement from the nested, basement crater, we here make a full lithological description of the Lockne-9 core section and a precise analysis of the rock magnetic properties from the core and reference samples from both within the and beyond the area affected by the impact. This work also addresses the effect of post-impact hydrothermal alteration on the magnetic properties of core samples in terms of coercivity, unblocking temperature, saturation of the isothermal magnetization, and hysteresis ratios.

2. Methodology

Laboratory measurements of rock magnetic properties were made on samples of different lithologies of the Lockne-9 core. This core was drilled in 2004 and is now stored at Centro de Astrobiología (CAB), Spain. Rock magnetic measurements were done both at CAB

and in the Paleomagnetism Laboratory of the Physics Faculty at the Complutense University, Madrid. Additionally, geochemistry and lithological descriptions have been made to support the interpretations of the petrophysical results, which include X-ray fluorescence (XRF) spectrometry, thermogravimetric (TGM) analysis and scanning electron microscopy in combination with Energy Dispersive X-ray spectroscopy (SEM-EDX).

2.1. Lithological analysis of the drill core

The 31.04 m long drill core, which is 4.2 cm in diameter, is almost complete except for a loss of the uppermost 2.27 m. A macroscopic description of lithological and structural features has been combined with thin sections and SEM-EDX analysis in some selected parts.

2.2. Rock magnetism

The magnetic susceptibility of the whole core (425 measurements) was measured in 3–5 cm intervals with a SatisGeo KT-6 field kappameter wherever core conditions allowed it (pieces larger than 10 cm). This susceptibility meter operates at 10 kHz frequency, and it has a 1×10^{-5} [SI] sensitivity. In order to reduce the possible external errors because of the cylindrical surface, each point was measured three times and an average value was calculated. A correction factor 2 from the instrument provider was applied depending on the diameter of the core.

A total of 88 samples with masses between 0.8 and 2.5 g were cut from the core in order to measure both induced and remanent magnetization in a coercivity spectrometer J_Meter (Jasonov et al., 1998). Initial magnetization curves, hysteresis loops, acquisition of isothermal remanent magnetization curves (IRM), and further backfield static demagnetization curves were obtained with this instrument up to a maximum field of 500 mT. We developed a Matlab routine in order to extract the magnetic parameters out of the coercivity spectrometer measurement. For a more detailed explanation of the magnetic parameters, their determination and significance see Dunlop and Özdemir (1997), and references therein.

The slope of the initial magnetization curves, or low-field susceptibility, is dominated by the ferromagnetic minerals. The induced magnetization of para/diamagnetic minerals in this range (0–50 mT) can be neglected (Dunlop and Özdemir, 1997). The slope of the hysteresis curve after the saturation of the ferromagnetic phases is due to the para/diamagnetic minerals in the rock and was measured as a proxy for their characterization within the rock.

The hysteresis measurement allowed the determination of the saturation magnetization (M_s), remanent magnetization (M_r) and magnetic coercivity (H_c). Backfield curves were used to compute the coercivity of remanence (H_{cr}).

IRM curves help to identify the different magnetic fractions depending on the field at which saturation is reached (Butler, 1992). The derivative of the IRM curve can also be used to fully characterize the number and nature of ferromagnetic phases, the so-called coercivity spectral analysis. There are several methods as well as software to perform that analysis (Egli, 2004a; Heslop et al., 2002; Kruiver et al., 2001). Because of the simplicity of the initial assumptions, we here choose the method developed by Kruiver et al. (2001), which can be used in an Excel spreadsheet. The IRM gradient is fitted into a series of log-normal distributions. The central point of each normal distribution is an indicator of the average coercivity of the population, and its standard deviation is an estimation of the uncertain of this property. Each normal distribution with different features indicates fractions with different properties, either due to the same composition but different characteristics or due to differences in the composition.

Thermomagnetic measurements were carried out to characterize the contributing magnetic minerals. Thirty-six samples of 100 to

260 mg were taken from every lithology on the core. Samples were heated up to 700 °C with saturating field of a 1 T with the aim of determining the Curie/Neel temperature. These measurements were carried out in a Variable Force Translation Balance High-sensitivity Magnetometer (VFTB manufactured by Petersen Instruments).

2.3. XRF Spectrometry

The XRF spectrometric analysis were done for a total of 26 samples from the various lithologies of the Lockne-9 core. The samples were analysed in a wavelength dispersive sequential X-ray spectrometer PHILIPS PW2404 at the University of Oviedo (Spain). In this study, we have considered the simplified model that assumes SiO₂ content as an indicator of diamagnetic/paramagnetic materials and Fe₂O₃ and TiO₂ as indicators of the ferrimagnetic behavior within the different lithologies of the Lockne-9 core.

3. Results

3.1. Core log description

Based on macroscopic observations of the core, and to facilitate the comparison with the petrophysical results, we have divided the core into three main lithological sections: the crystalline ejecta, a zone of mixing between ejecta and preserved parts of the target, and the autochthonous basement (Fig. 2).

3.1.1. Crystalline ejecta

The crystalline ejecta in the core consists mainly of a brecciated, dark grey, mafic rock, which in the upper 11.40 m of the breccia is of medium grain size and shows an ophitic texture that gradually disappears downward (grain size graph in Fig. 2). The fragments of the breccia are rotated, angular to subrounded, and occur in a dark matrix. The breccia

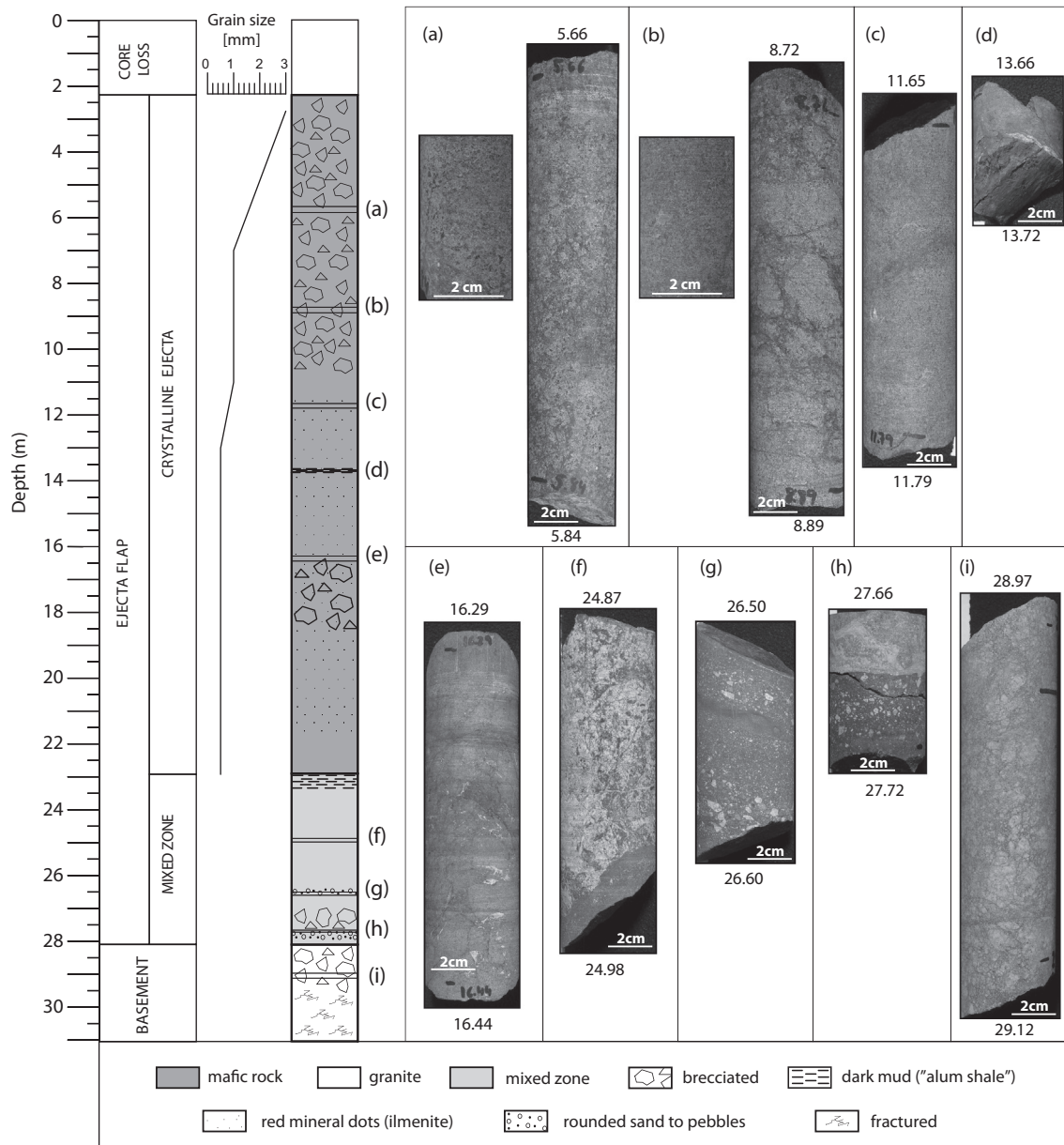


Fig. 2. Core log of the Lockne-9 drill core with photos of representative lithologies discussed in the text.

becomes increasingly matrix supported downward, and in some parts clasts show a very good fitting. The clast size varies from a few millimeters up to 3–4 dm with dominance of the larger fraction (Fig. 2b). The ophitic texture of the clasts also shows frequent millimeter sized black minerals (likely pyroxene) that decrease in frequency to 8 m depth (Fig. 2a, magnified picture).

At around 11.40 m depth, a transition to a more fine grained, dark, greenish mafic rock occurs. This part of the core shows a microbreccia with clasts size of about 0.5–2 cm (Fig. 2c). Even brecciated larger clasts occur giving the impression of a “breccia in breccia.” Common sub-millimeter sized dots of a red mineral appear at 11.70 m and with increasing amount downward in the core until they disappear at 21.80 m (Fig. 2c, magnified picture). According to our SEM-EDX analysis, this is a titanium-iron mineral, most likely ilmenite (see supplementary material). The ilmenite growth seems to be secondary as it overprints the microbreccia. The generally dark matrix passes into dark shale between 13.60 m and 13.72 m (Fig. 2d). An origin from Cambrian alum shale is inferred from U-Th rich bitumen nodules previously observed in the core (Lindgren et al., 2007). The micro-breccia is most obvious in the transitional part, to the coarser rock (11.40 to 14.40 m). Below this interval of the core, the greenish mafic rock is very fine grained and any brecciation is hard to distinguish, although

some disintegration is visible between 16.30 m and 18.80 m (Fig. 2e). From 18.80 m downward, the material is again more obvious clast supported breccia with subrounded clasts reaching sizes up to some centimeters within a fine grained, black matrix.

3.1.2. Mixed zone

Sandwiched between the mainly mafic crystalline ejecta and the granitic basement is a mixed zone of both mafic and granitic breccia clasts blended with sediments from the Palaeozoic target sequence. This mixed zone starts at 22.90 m depth with 50 cm of dark mudstone (i.e., Cambrian alum shale). It is followed downward by a granitic breccia between 23.40 m and 26.40 m, (Fig. 2f). The clasts are angular with good fitting. Some well-rounded crystalline pebbles occur in the otherwise black matrix. Thus, a provenance from the Lower Cambrian conglomerate of the target succession is most likely. At 26.40 m, there is a 20 cm thick section of dark matrix that show fractioning of the grain sizes from silt at the contacts to the surrounding breccia blocks, to gravel in its central part (Fig. 2g). The dark mud and the pale, weathered fragments in the coarser fraction suggest a provenance from the Cambrian conglomerate. However, the size sorting indicate emplacement as an injection (cf. injected dikes described by Sturkell and Ormö, 1997). The core continues downward with a blend of granitic breccia, often

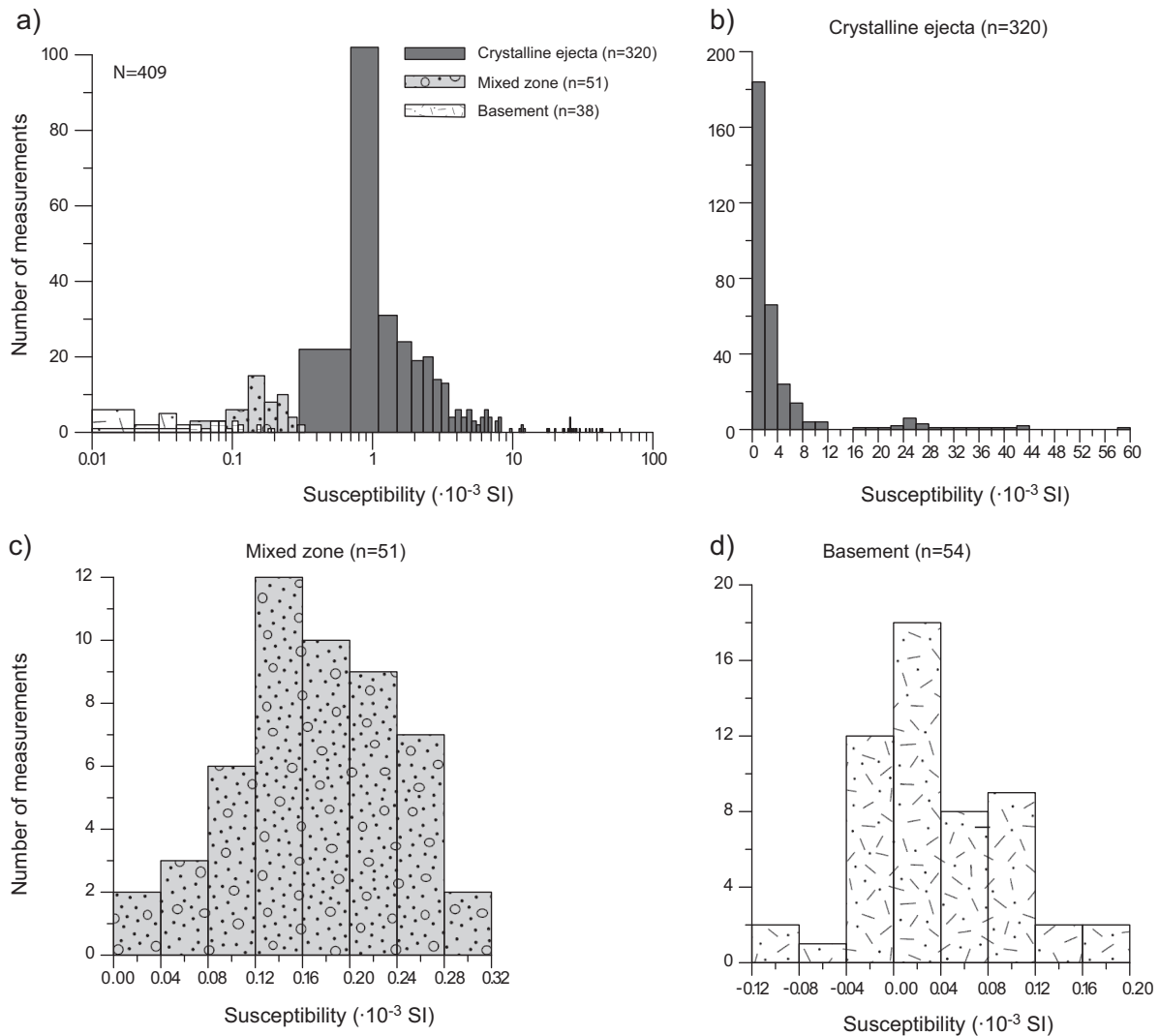


Fig. 3. Histograms of magnetic susceptibility obtained with a KT-6 hand susceptometer for the three main lithological sections of the Lockne-9 core: (a) a logarithmic histogram comparing the three major lithologies. In the logarithmic histogram 16 negative or zero values had to be removed by the logarithm definition, (b) crystalline ejecta, (c) mixed zone, and (d) fractured basement.

with dark matrix, and dm-thick sections of alum shale. In Fig. 2h, the contact between clast supported, granitic breccia (top) at 27 m depth and 22 cm of reworked Lower Cambrian conglomerate (bottom) is displayed. It shows similarities to the occurrence shown in Fig. 2g at 27.67 m depth.

3.1.3. Basement

The breccias and reworked sediments of the ejecta and the mixed zone rest at 28.10 m depth on fractured and brecciated basement with a sharp contact. This depth coincides with the estimated level of the sub-Cambrian peneplain (Ormö and Lindström, 2005; Sturkell and Lindström, 2004). The dominantly light grey granitic rock of the basement is in strong contrast to the overlying mafic rocks of the ejecta and continues to the end of the core at 31.04 m depth. The basement is strongly brecciated (Fig. 2i), mostly clast-supported with good fitting, but locally matrix-supported with rotated clasts of a few millimeters up to a decimeter in size in a dark matrix.

3.2. Bulk rock magnetic properties

Fig. 3 shows histograms that summarize the measured susceptibility values. The highest susceptibility values are observed in the middle part of the crystalline ejecta. The peak value is 58.2×10^{-3} [SI] to be compared with the minimum value of -0.10×10^{-3} [SI] measured in the granitic fractured and brecciated basement (Fig. 3a and Fig. 3d). Thus, there is a clear difference between the crystalline material of the ejecta flap and the basement. Obtained values correlate well with previous measurements in corresponding lithologies of the Lockne impact crater (Törnberg and Sturkell, 2005). The crystalline ejecta low-field susceptibility follows a bimodal distribution of values, with a narrow population with values in the order of 10^{-3} [SI] and a second population of higher and wider susceptibility range (Fig. 3b). This second population has magnetic susceptibility values between 16×10^{-3} [SI] and 44×10^{-3} [SI], which means two or three orders of magnitude higher than the rest of the core. The mixed zone has susceptibility in the

order of 10^{-4} [SI] (Fig. 3c). Negative susceptibility values for material from the fractured and brecciated granitic basement may correspond to a diamagnetic material, most likely with high abundance of quartz and feldspar (Fig. 3d).

We observed three different types of hysteresis loops depending on the main carrier of the magnetic signal: (i) dominated by the paramagnetic fraction, (ii) dominated by the ferromagnetic phases, or (iii) mixed by the two types of magnetic minerals (Fig. 4). The upper part of the core displays a mixed composition, with a significant paramagnetic contribution to the magnetization curve and a closed hysteresis loop (Fig. 4a). After subtraction of the paramagnetic signal, the hysteresis reaches saturation at approximately 250 mT and displays an open loop. The hysteresis loops dominated by the ferromagnetic fraction are found mainly in the upper part of the transition to the more fine grained, greenish, mafic rock in the ejecta flap (between 11.40 and 12.50 m) with almost no contribution of the paramagnetic fraction (Fig. 4b). The lower part of the core section, from 22.90 m to the end, corresponding to the mixed zone (Fig. 4c) and the basement (Fig. 4d), is dominated by the paramagnetic/diamagnetic fraction. After the paramagnetic correction, the hysteresis loops show an almost closed loop with very low coercivity. Therefore, magnetic susceptibility derived from hysteresis loops is consistent with low-field susceptibility measurements obtained with a KT-6 hand susceptometer shown in Fig. 3. In all analyzed samples, the hysteresis loop reaches saturation at 250 mT, although the saturation magnetization varies with the lithology. The coercivity (between 5 and 21 mT), the coercivity of remanence (between 17 and 92 mT), and the field at which saturation is reached suggest the presence of magnetite/titanomagnetite (Dunlop and Özdemir, 1997).

Three typical IRM acquisition curves have been obtained along the core (Fig. 5). Saturation is reached at about 250 mT in samples with the type of curves represented by Fig. 5a. This result suggests the presence of magnetite/titanomagnetite in these type of samples (Lowrie, 1990). Several samples show a different behavior with saturation that is not reached at 500 mT (Fig. 5b). The high coercivity suggests the

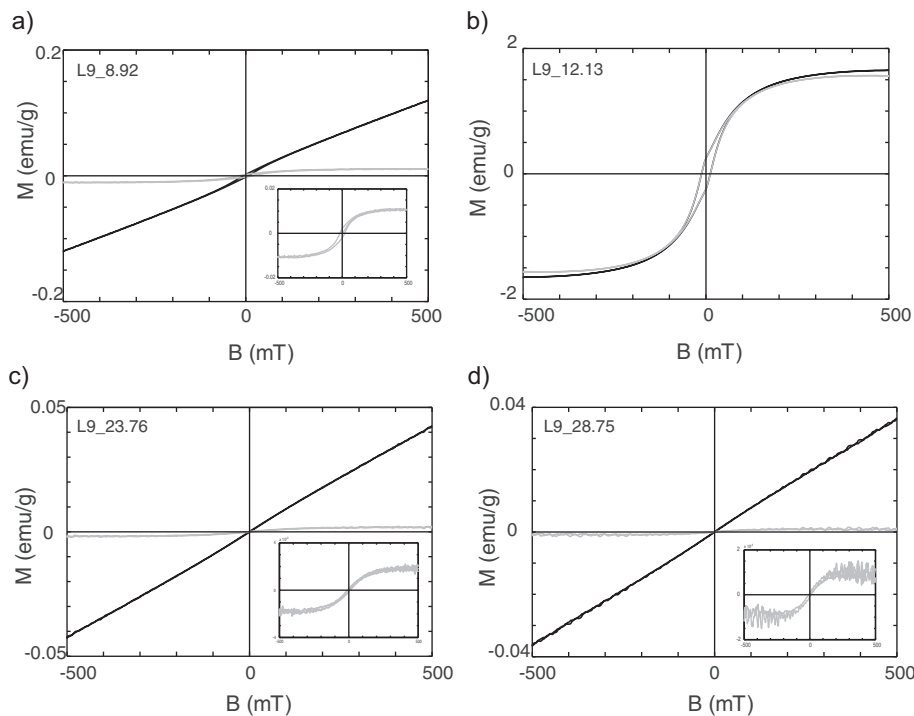


Fig. 4. Typical hysteresis loops obtained from the three main lithologies in the Lockne-9 core. The black curve represents the measured hysteresis and the grey curve represents the hysteresis corrected by the paramagnetic susceptibility. The inset shows a magnified part of the corrected hysteresis loop. Graphs a and b represent loops obtained from the crystalline ejecta flap, graph c shows typical loops for the mixed zone, and graph d shows loops for the granitic basement. Graph a shows mixed loops with contribution from both paramagnetic and ferromagnetic fraction, graph b shows loops dominated by the ferromagnetic fraction, and graphs c and d show loops dominated by the paramagnetic fraction.

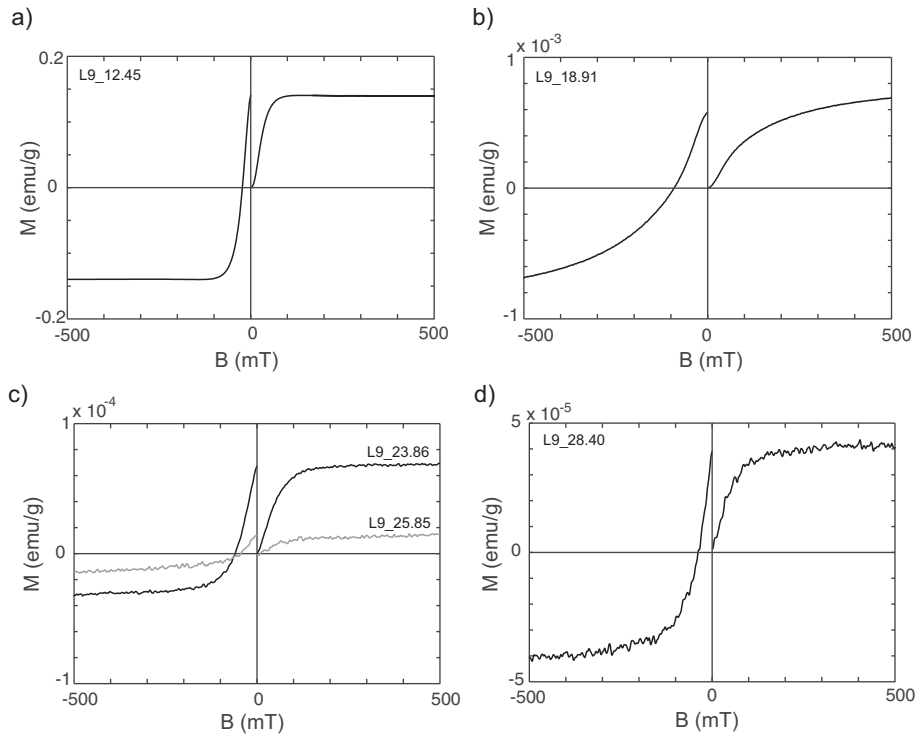


Fig. 5. Typical IRM acquisition and back field demagnetization curves from the different lithologies of Lockne-9 core. Graphs a and b show curves obtained for the crystalline flap, graph c shows two curves represented in black and pale grey obtained for the mixed zone, and graph d shows a curve obtained for the granitic basement. Graph a and c (black curve) show IRM curves reaching saturation at 250 mT approximately, graph b shows an IRM curve that did not reach saturation for the maximum field applied, and graphs c (pale grey) and d show mixed curves with contribution from a fraction that reached saturation at 250 mT and one that did not reach saturation.

presence of a high coercivity mineral, most commonly goethite or hematite (Lowrie, 1990). The rest of the samples show a mixed curve with a fraction saturating at 250 mT and another fraction that not reaches saturation (Fig. 5c and d).

The coercivity spectra of a total of 36 characteristic samples were analyzed following the protocol described by Kruiver et al. (2001) and is displayed in three selected characteristic curves in Fig. 6. Twenty-four samples display an IRM acquisition curve dominated by one population of magnetic minerals, and therefore, the corresponding coercivity spectra is also dominated by one main function (Fig. 6a and Fig. 6c). This spectrum has a main normal distribution centered at 1.50 mT and with a 0.25 dispersion parameter value, which is the main carrier of the signal. This type of IRM coercivity spectra is observed mainly in the crystalline

ejecta. Additionally, it has been necessary to include one population with low median destructive field ($B_{1/2} = 10$ mT) and a dispersion parameter ($DP = 0.28$) that contributes less than 15% of the signal. Some authors have attributed this to thermal activation processes of the magnetic particles (e.g., Heslop et al., 2004). In some samples of this type, at high coercivities, also a minor distribution has been included that contributes with less than 5%, which is considered to be a mathematical artifact due to the instrumental noise at high fields. Twelve samples displayed an IRM acquisition curve that did not saturate at 500 mT. The corresponding coercivity is fitted into a distribution with two different components of similar intensity (Fig. 6b). This high coercivity population contributes with 20–64% of the signal depending on the sample, with high median destructive field of $B_{1/2} = 501.2$ mT

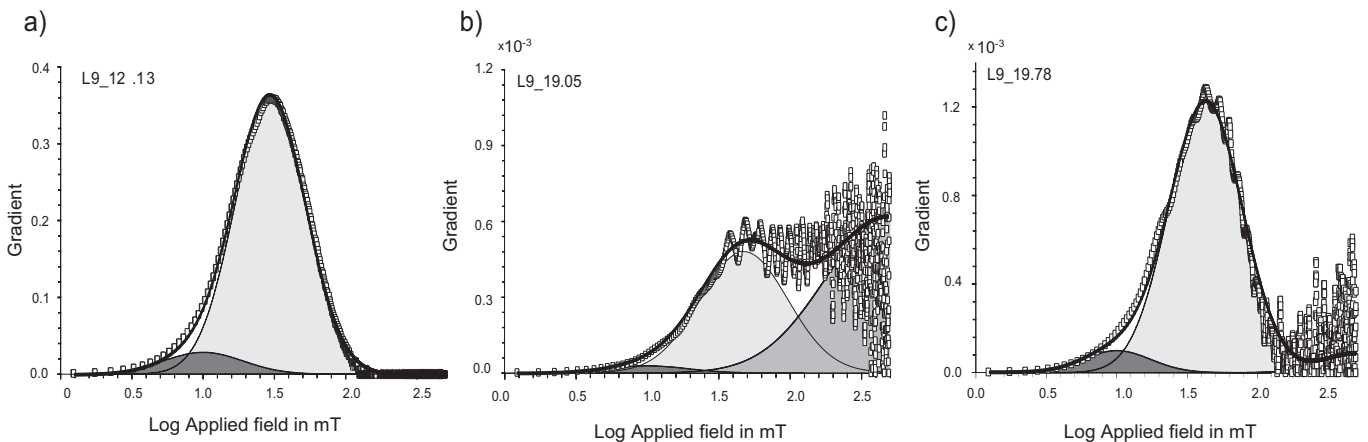


Fig. 6. Derivatives of the IRM curves (white symbols) with the corresponding modeled curve derived from the fitting into a series of Gaussian distribution of coercivity-derived curves (thickest black curve). Individual components of the different magnetic fractions and coercivity distributions are shown as grey shadowed areas for the three examples.

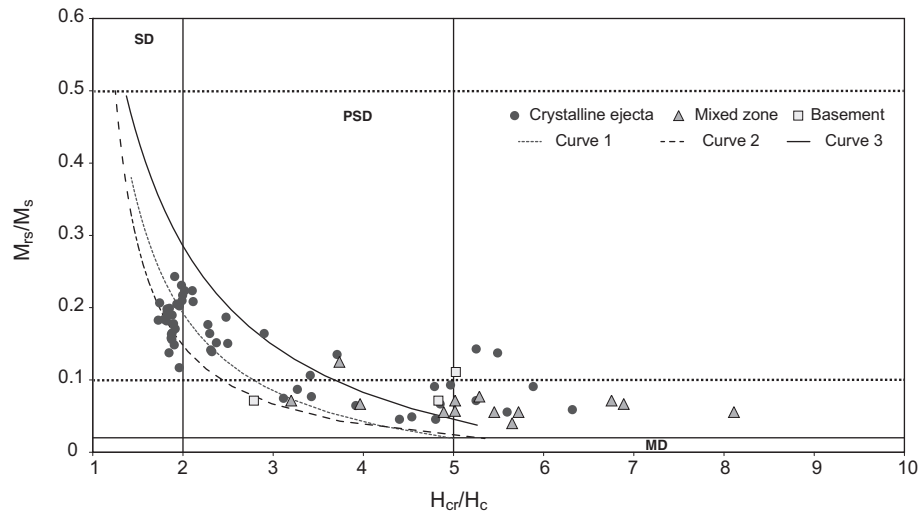


Fig. 7. Day plot summarizing magnetization ratios M_{rs}/M_s as a function of coercivity ratios H_{cr}/H_c (Day et al., 1977) for the three studied lithologies where the significance of the symbols appears in the legend. Curves 1, 2, and 3 correspond to mixture models proposed by Dunlop (2002a, 2002b).

and a dispersion parameter $DP = 0.45$. Moreover, it is necessary to include the low coercivity population attributed to the thermal activation process of the particles.

A summary of the domain state can be visualized in a Day plot (Day et al., 1977). The coercivity ratios as function of the magnetization ratios are a proxy of the domain state. The ratios were described later as a mixture of two end-members of single domain (SD) and multidomain (MD) particles giving rise to theoretical mixture curves (Dunlop, 2002a, 2002b). Fig. 7 shows that several samples from the crystalline ejecta plot within the pseudo-single domain region (PSD), and it corresponds to a mixture with 50% contribution from single domain grains and 50%

from pseudo-single domain fraction. A gradual increase to the MD region with depth is observed with the exception of samples from the granitic basement which plot at boundary between PSD and MD fields.

Thermomagnetic curves have been analyzed for 36 samples from the drill core. Because thermal methods lead to the destruction of the material only representative samples have been measured. The Curie temperature of the ferromagnetic phases has been determined by using the second derivative method (Moskowitz, 1981). Fig. 8a shows a characteristic thermomagnetic curve obtained from samples located in the crystalline ejecta. The heating curve indicates a first inflexion of the curve around 100 °C, and the cooling curve presents a second

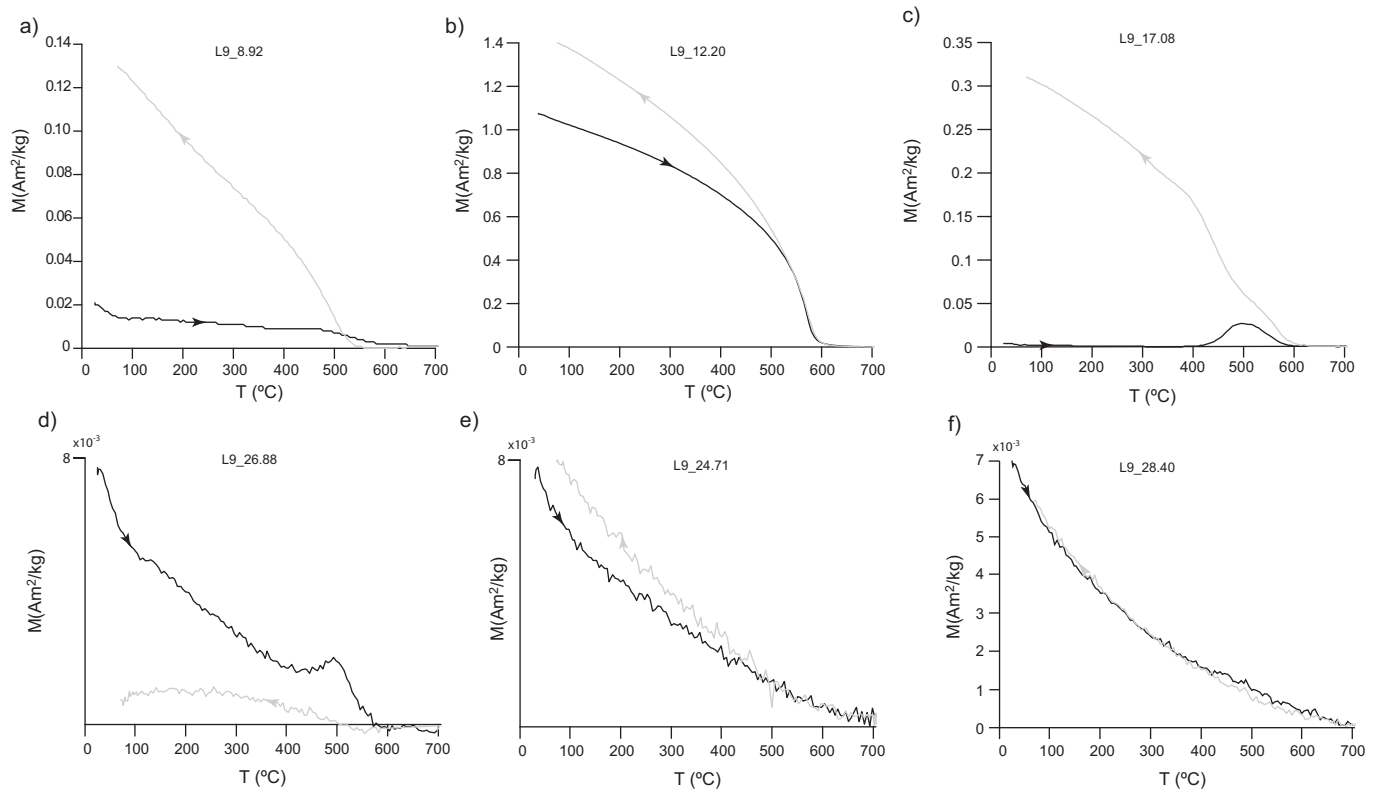


Fig. 8. Characteristic thermomagnetic curves obtained from the three main lithologies of Lockne-9 core where black indicates the heating curve and pale grey indicates the cooling measurements. Graphs a, b, and c show thermomagnetic curves obtained for the crystalline ejecta flap, graphs d and e show two representative curves obtained for the mixed zone, and graph f shows thermomagnetic curves for the granitic basement.

Curie temperature value around 525 °C that could be attributed to titanomagnetite with a low Ti content (O'Reilly, 1976). The upper part of the transition to the more fine greenish mafic rock, between 11.40 and 12.50 m, is evident in the thermomagnetic curves (Fig. 8b). For these samples, the heating curve indicates an initial presence of a ferromagnetic fraction, and the cooling curve reveals a Curie temperature around 580 °C corresponding to magnetite (Dunlop and Özdemir, 1997). The cooling curve in Fig. 8b shows an initial part of total overlap

revealing a reversible behavior, and the following higher demagnetization temperature indicates slight alteration of the initial features. Fig. 8c represents a thermomagnetic curve of a sample from the crystalline ejecta enriched in pyrite. Evidence of pyrite transformation between 400 and 600 °C in the heating transect (black curve) described in previous studies (e.g. Mullender et al., 1993; Tudryn and Tucholka, 2004) is clearly observed. Fig. 8d shows one of the two different types of thermomagnetic curves obtained from the mixed zone. The heating

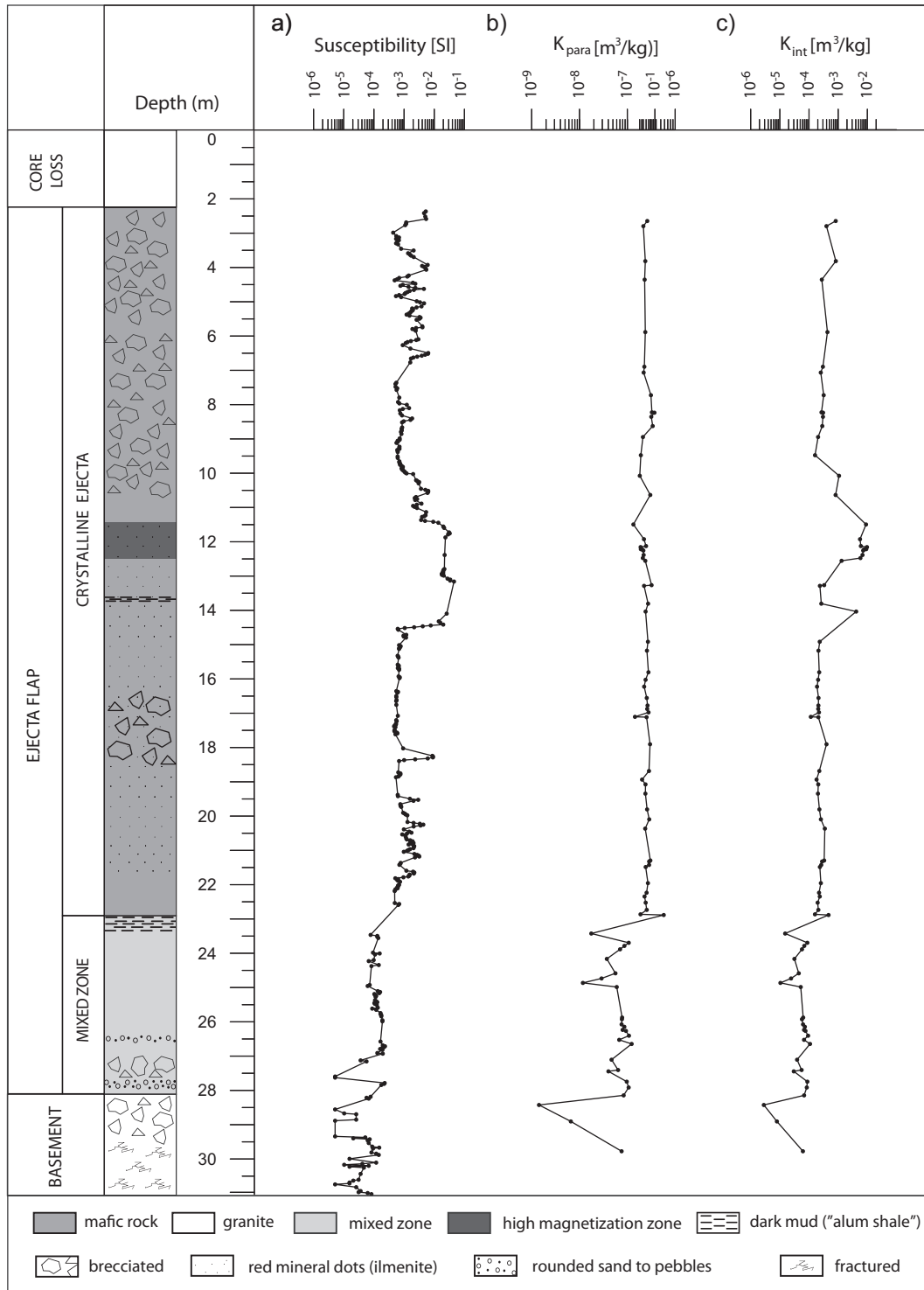


Fig. 9. Representation of the dependence of the different susceptibility results obtained by different methods along the Lockne-9 drill core. Graph a shows susceptibility measurements obtained with a KT-6 field susceptimeter, graph b shows the paramagnetic susceptibility obtained from the coercivity spectrometer (J_Meter) measurements, and graph c shows initial susceptibility obtained from the coercivity spectrometer (J_Meter) measurements.

measurements show an unblocking temperature around 100 °C and a local maximum centered on 500 °C. This last feature indicates the presence of an important paramagnetic fraction of pyrite. On the other hand, the other type of curves obtained from the mixed zone as well as the samples from the fractured and brecciated basement (Figs. 8c and d) show thermomagnetic curves where both heating and cooling curves are very noisy and the paramagnetic materials dominates the magnetic signal.

Many of the thermomagnetic curves analyzed from the ejecta flap present a decrease in the magnetization of the heating curve around 100 °C (Fig. 8a and d). When this inflexion is related to the unblocking temperature of a ferromagnetic phase, the most likely mineral to support this behavior would be goethite. It has a Curie temperature of 120 °C that can be decreased by a number of factors such as low crystallinity, stoichiometry, higher water content, or inclusion of elements such as Al (Dekkers, 1988). In order to corroborate the presence of goethite, additional thermogravimetric analyses (TGA) have been carried out in six significant samples (see complementary material) finding no signs of goethite dehydroxylation in the weight or heat loss flow with temperature. These analyses conclude that goethite is not present in these samples.

3.3. Depth-dependent rock magnetic properties

Fig. 9a represents the low-field susceptibility as a function of depth. Values are very similar along the profile with the exception of levels between 11.40 and 14.40 m approximately, which coincides with the transition to the more fine grained greenish variety of the mafic rock. As shown by the susceptibility histograms in Fig. 3, a decrease in susceptibility values within the mixed zone and the basement is very clear. Paramagnetic susceptibility computed as the slope of the hysteresis loop above saturation of the ferromagnetic phases can be seen in Fig. 9b. Samples from the crystalline ejecta hardly show any variations of paramagnetic susceptibility as a function of depth. This indicates a homogeneous composition within this lithology. A very clear decrease in paramagnetic susceptibility is observed in the mixed zone and the fractured basement as a consequence of an increasing content of granite. The fractured basement shows low values close to the diamagnetic boundary. Fig. 9c shows the initial susceptibility profile calculated as the slope of the initial magnetization at low values of the field. The initial susceptibility is mainly due to the ferromagnetic minerals. The signal is very homogeneous along the profile with the exception of a maximum between 11.40 m and 14.40 m. This zone correlates to the maximum observed in the bulk susceptibility profile (Fig. 9a) and corresponds to the transition to the more fine grained greenish variety of the mafic rock. These profiles suggest that this part of the crystalline ejecta present an increase of the ferromagnetic content. Comparing the content of the major elements from Table 1, there is not a very obvious difference in values within the crystalline ejecta lithology although the highest values of TiO₂ and Fe₂O₃ are found in this high susceptibility zone.

Fig. 10 shows the hysteresis parameters as a function of depth. Magnetization parameters (Fig. 10a and b) have a similar behavior with almost constant values of about $M_s = 10^{-2}$ Am²/kg and $M_r = 10^{-3}$ Am²/kg with the exception of the levels between 11.40 and 12.50 m where there is an increase in both parameters. This is a similar behavior as observed in the initial susceptibility (Fig. 9b) and in the bulk susceptibility (Fig. 9c). This happens in the transition to the more fine grained greenish variety of the mafic rock in the crystalline ejecta. The coercivity parameters (Fig. 10c and d) show a similar trend, and ranges between $H_c = 5$ mT and $H_c = 20$ mT. Samples from the crystalline ejecta present high coercivity values of about 15 mT that decreases downward reaching a minimum at about 12 m. This minimum corresponds to the maximum in M_s and M_r already described. This lithology presents the more complex behavior in terms of coercivity. It has a maximum at 13.26 m following by the absolute minimum of the

core at 17 m and recovers high values of about 21 m toward the end of the lithology. The values of coercivity of the mixed zone and the fractured basement show a slowly decreasing trend. The highest ratios of M_r/M_s are reached in the flap (Fig. 10e). A notable decrease is observed along the depth of the core, but in two zones of the crystalline ejecta (between 11 and 15 m and between 20 and 22 m), high ratios are reached (between 0.20 and 0.24 approximately). The lowest values are obtained in the lower part of the core (from 23 to 31 m). The ratio between H_c and H_{cr} ranges from 1 to 3 along almost the whole crystalline ejecta, but a zone stand out with high ratio between 15 and 19 m approximately (Fig. 10f). This ratio increases in the mixed zone and fractured basement reaching values from 3 to 5. It is important to emphasize the inverse relationship between these two ratios in the main trend and in several small peaks (as the ones observed at 8, 9 and 10 m approximately).

3.4. Geochemical data and their correlation with rock magnetic properties

Major element data are listed in Table 1. Fig. 11 shows the relations between the most relevant major elements measured: Fe₂O₃ versus SiO₂ (Fig. 11a), TiO₂ versus SiO₂ (Fig. 11b) and Fe₂O₃ versus TiO₂ (Fig. 11c). A clear grouping of values is observed, i.e., a first group (group 1) is dominated by the mafic rock of the crystalline ejecta and a second group (group 2) is dominated by the mainly felsic rocks of the mixed zone and the fractured basement. Samples belonging to group 1 present low SiO₂ and higher Fe₂O₃ and TiO₂. The opposite behavior is observed in samples from group 2 with higher SiO₂ and lower Fe₂O₃ and TiO₂ content.

Fig. 12 shows the relations between the most relevant major elements and some of the magnetic parameters obtained by the rock magnetic analysis described above. Figs. 12a, b and c represent the relationship between the paramagnetic susceptibility and the SiO₂, Fe₂O₃ and TiO₂ content respectively. The same grouping as described above for Fig. 11 is found also in this plot. High paramagnetic susceptibility is observed in samples from group 1 together with high Fe₂O₃ and TiO₂ contents suggesting that Fe and Ti are present within the lattice of paramagnetic minerals (cf. Rochette, 1987) (Fig. 12b and c).

Table 1
Major elements content from Lockne-9 core samples.

Depth (m)	SiO ₂ (%)	Fe ₂ O ₃ (%)	TiO ₂ (%)	Al ₂ O ₃ (%)	CaO (%)	MnO (%)	K ₂ O (%)	MgO (%)	Na ₂ O (%)	P ₂ O ₅ (%)
4.33	42.13	15.92	1.99	14.45	5.47	0.31	1.18	9.91	1.67	0.23
7.70	40.80	16.38	2.20	13.73	4.91	0.32	0.84	10.81	1.72	0.24
8.60	38.93	14.26	1.34	13.22	10.01	0.27	0.60	9.35	1.44	0.17
10.61	41.84	15.65	1.91	10.75	7.68	0.25	0.55	9.88	1.24	0.26
12.30	45.38	14.57	2.22	16.65	2.68	0.16	2.59	8.47	1.87	0.25
12.45	45.17	14.58	2.24	16.73	2.34	0.18	3.50	8.02	1.80	0.26
12.81	45.59	16.47	2.67	14.57	1.73	0.17	3.79	8.34	1.63	0.33
13.24	41.60	17.30	2.18	15.05	1.97	0.14	2.83	7.92	1.04	0.25
15.22	42.17	13.49	1.93	14.26	8.57	0.19	0.62	9.57	0.26	0.21
15.44	42.09	13.33	1.88	14.02	8.42	0.18	0.63	9.5	0.26	0.21
16.13	44.53	13.52	2.07	15.76	9.32	0.14	0.44	8.08	0.07	0.24
16.53	34.83	14.15	1.90	17.49	8.52	0.17	0.76	12.33	0.05	0.24
18.66	40.81	14.93	2.09	15.96	6.64	0.17	0.38	11.38	0.07	0.28
19.03	47.95	13.77	2.10	15.80	2.17	0.15	2.47	7.31	2.04	0.23
19.05	48.60	13.05	2.13	15.75	1.95	0.14	2.84	7.02	1.90	0.23
20.34	43.40	15.42	2.07	15.70	1.89	0.20	2.59	10.07	1.29	0.27
21.39	42.77	14.46	2.12	16.58	3.08	0.17	3.41	8.57	1.82	0.25
21.43	43.00	12.92	2.13	16.13	4.12	0.15	3.59	7.68	2.02	0.24
22.24	40.22	16.34	2.29	17.51	1.77	0.15	2.30	10.54	1.27	0.26
23.86	54.68	3.96	0.33	19.08	2.55	0.08	3.94	6.40	0.07	0.03
24.71	56.15	3.67	0.24	19.08	2.69	0.08	4.41	6.09	0.08	0.03
26.12	58.49	4.72	0.18	16.64	2.72	0.09	2.92	6.88	0.07	0.06
27.42	64.08	2.69	0.14	15.62	1.60	0.04	5.52	4.00	0.81	0.03
27.89	50.34	6.52	0.52	18.82	2.65	0.10	5.28	7.46	0.44	0.10
28.72	63.39	0.77	0.14	18.77	2.40	0.02	0.45	0.54	10.25	0.03
29.75	59.00	4.23	0.37	18.99	2.25	0.05	5.89	2.76	2.97	0.07

Bold indicates the samples within the high susceptibility zone.

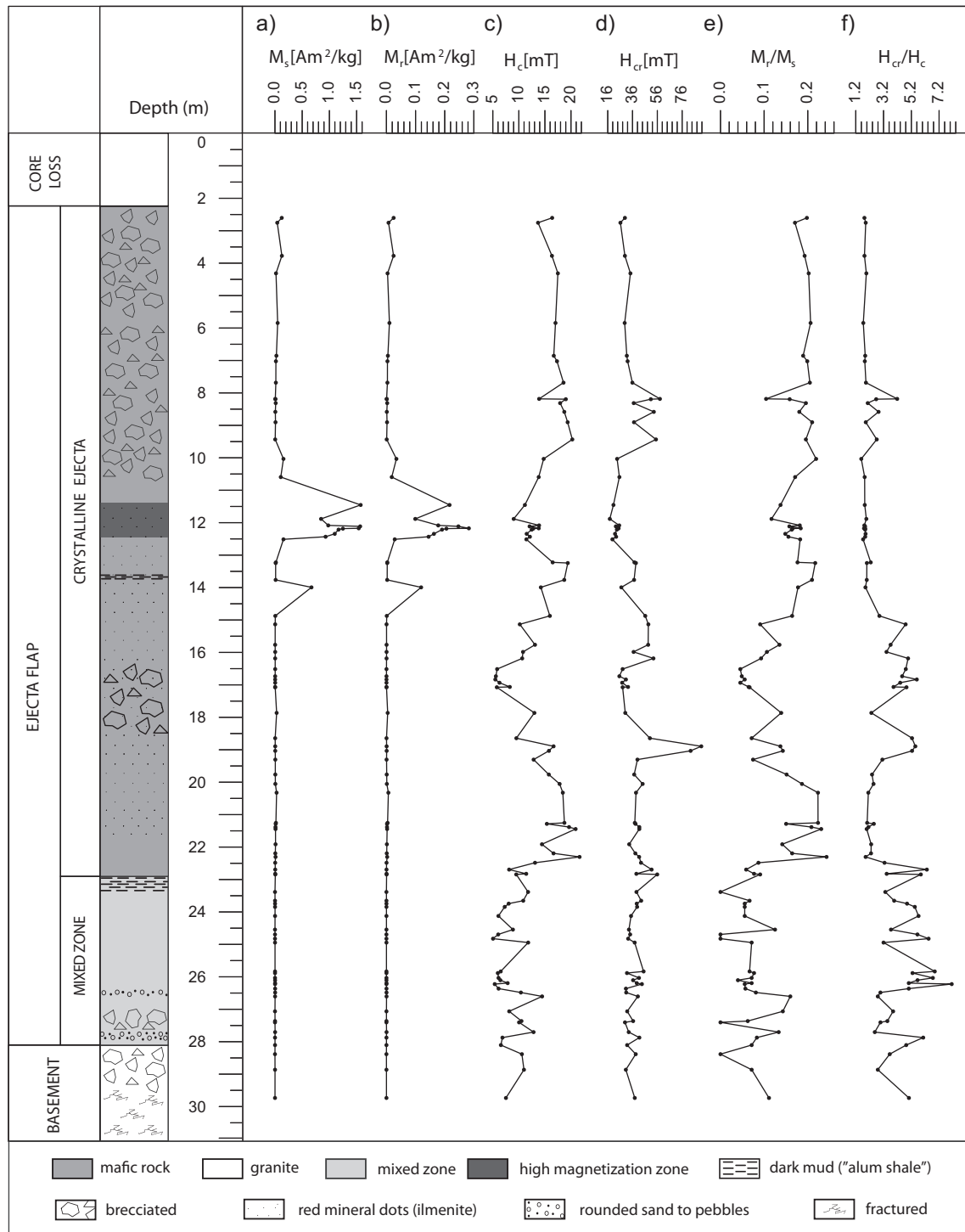


Fig. 10. Representation of the dependence of the different magnetization and coercivity results obtained from the coercivity spectrometer (J_Meter) measurements with depth on the Lockne-9 drill core. (a) Saturation magnetization, (b) remanent magnetization, (c) magnetic coercivity, (d) coercivity of remanence, (e) magnetization ratio M_r/M_s , and (f) the coercivity ratio H_{cr}/H_c .

The relationship between these element concentrations and the ratio between M_s and M_r is shown in Fig. 12d, e and f. The distinction of the two main lithological groups is also observed in these plots. The same behavior as observed in the paramagnetic susceptibility is seen also for the ratio M_s/M_r in relation to the SiO_2 , Fe_2O_3 and TiO_2 content. However, three samples from the ejecta flap show lower magnetization ratios. These samples correspond to singular minimum peaks observed between 15 and 19 m depth in Fig. 10e. Figs. 12g–i show the relation between the ratio H_{cr}/H_c and the SiO_2 , Fe_2O_3 and TiO_2 content. The

coercivity ratio is a less sensitive parameter to the cation content in this case, and the general classification into the two groups cannot be applied here.

3.5. Rock magnetic properties of unshocked dolerite

We have compared the measurements from the high magnetization zone obtained from the rock magnetic study in Lockne-9 core (from 11.40 to 12.50 m) with three samples taken from different dolerite

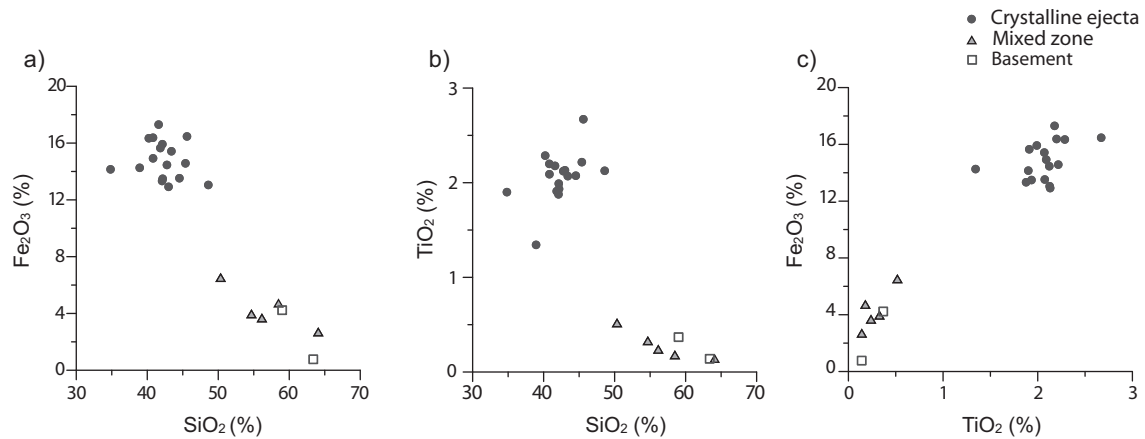


Fig. 11. Geochemical discrimination diagrams for the crystalline ejecta, mixed zone and granitic basement. (a) Fe₂O₃ vs. SiO₂, (b) TiO₂ vs. SiO₂, and (c) Fe₂O₃ vs. TiO₂ content of 25 samples from the Lockne-9 core. Each symbol represents a different lithology (see legend).

outcrops unaffected by the impact (Fig. 13 and Table 2). The locations of dolerite sampling sites in the close vicinity of the crater are shown in Fig. 1. In addition, one more reference sample was taken from a location (62°53'N 14°34'E) farther away from the crater. Comparison of the coercivity spectral analysis reveals a similar behavior of both affected and unaffected samples by the impact with a slight weakening of coercivity of the core samples (Fig. 13a). This property is also observed in the lower values of the median destructive field when compared with the SIRM (Fig. 13b). The Day plots of both types of samples are grouped in the same area although the coercivity ratio is higher in the core samples (Fig. 13c). Thermomagnetic curves represented in Fig. 13d reveal a unique unblocking temperature for all the samples corresponding to magnetite. However, the unblocking temperature obtained from the high magnetization zone of the ejecta flap is slightly higher than the unaffected samples from the dolerite outcrops.

4. Discussion

The rock magnetic properties together with the lithological observations of the Lockne-9 core can contribute to a better understanding of the ejecta flap formation mechanisms at the Lockne impact structure. Of special significance are two pieces of information: (i) typology of the ferromagnetic minerals and (ii) their location along the core.

The magnetic mineralogy of the investigated core is clearly related to the presence of magnetite/titanomagnetite particles (Figs. 4–8). In particular, the highest values of saturation magnetization obtained in the core are around 1.5 Am²/kg, and if we compare with the value for pure magnetite 92 Am²/kg (Dunlop and Özdemir, 1997), a magnetite content of 1.6% can be estimated. Hysteresis-derived parameters from the Lockne-9 core samples show a pronounced PSD behavior in the ejecta flap. As a consequence, the ferromagnetic phases found in this part of the core could slightly influence the values of the magnetic anomalies measured above the ground surface. On the other hand, the thermomagnetic curves reveal the presence of pyrite in some samples from the mixed zone (Fig. 8d) and in one sample from the crystalline ejecta at 17.08 m depth (Fig. 8c). The presence of pyrite has been observed in some samples extracted from impact breccia of the LOC5 core as well as in some localities in the vicinity of the crater (Angerer and Greiling, 2012; Sturkell et al., 1998a). Magnetite and titanomagnetite particles dominate the whole core with no traces of secondary minerals such as hematite. The fractured and brecciated basement stands out from the rest of the core with regard to the location of ferromagnetic minerals. Low or even negative susceptibility values were measured for this lithology as well as the mixed zone. This

indicates the presence of paramagnetic minerals (Fig. 3d). These results are supported by the thermomagnetic curves for samples from this part of the core (Fig. 8e and f). These observations imply that the redox conditions were not appropriate to form a significant amount of ferrimagnetic minerals during the impact.

In addition to the differences observed between the brecciated basement and the overlying mixed zone and crystalline ejecta is the conspicuous anomaly occurring between 11.40 and 12.50 m. Very high values in both bulk and also the initial susceptibility (Fig. 9a and c), and in the magnetization parameters (Fig. 10a and b) are obtained within the crystalline ejecta. This coincides with the transition from the coarser grained mafic rock to the finer grained greenish mafic rock inside the ejecta flap.

Two different possibilities for how to interpret this maximum are: either the values represent primary variations in the target before emplacement or the values represent alteration of the rock after the redeposition as impact ejecta. This second scenario would imply creation of new magnetic minerals, large variations in the magnetic grain size, and/or strong differences in the domain state. The rationale of the current results has been developed in the frame of the two possibilities based on three different rock magnetic experiments:

1. Coercivity spectra show only one significant component with a dispersion parameter (DP) of around 0.25 in the high magnetization zone (between 11.40 and 12.50 m), which suggests there was no transformation of the magnetic mineralogy as a consequence of the impact (Egli, 2004b).
2. Thermomagnetic curves from this part of the core show a Curie temperature of about 580 °C, which is a clear evidence of the presence of magnetite. Hysteresis loops and IRM acquisition curves support this result. In addition, thermomagnetic experiments show no evidence of hematite.
3. Consistency with the rock magnetic properties measured for dolerite sills within the crystalline basement at the crater. Comparison of the coercivity spectra reveals a similar behavior of the magnetic population between the high magnetization zone from the Lockne-9 mafic rock (11.40–12.50 m) and dolerite samples in the vicinity of the impact crater (Fig. 13a and b). The only observed discrepancy is a slight weakening in the coercivity of magnetic minerals of the core samples with respect to the rocks not affected by the impact (Fig. 13a and b). Thermomagnetic curves show a slight increase of the Curie point in samples of the core with respect to the unaffected samples (Fig. 13d). The report by Sturkell et al. (1998a) of low-temperature hydrothermal alteration associated with the impact

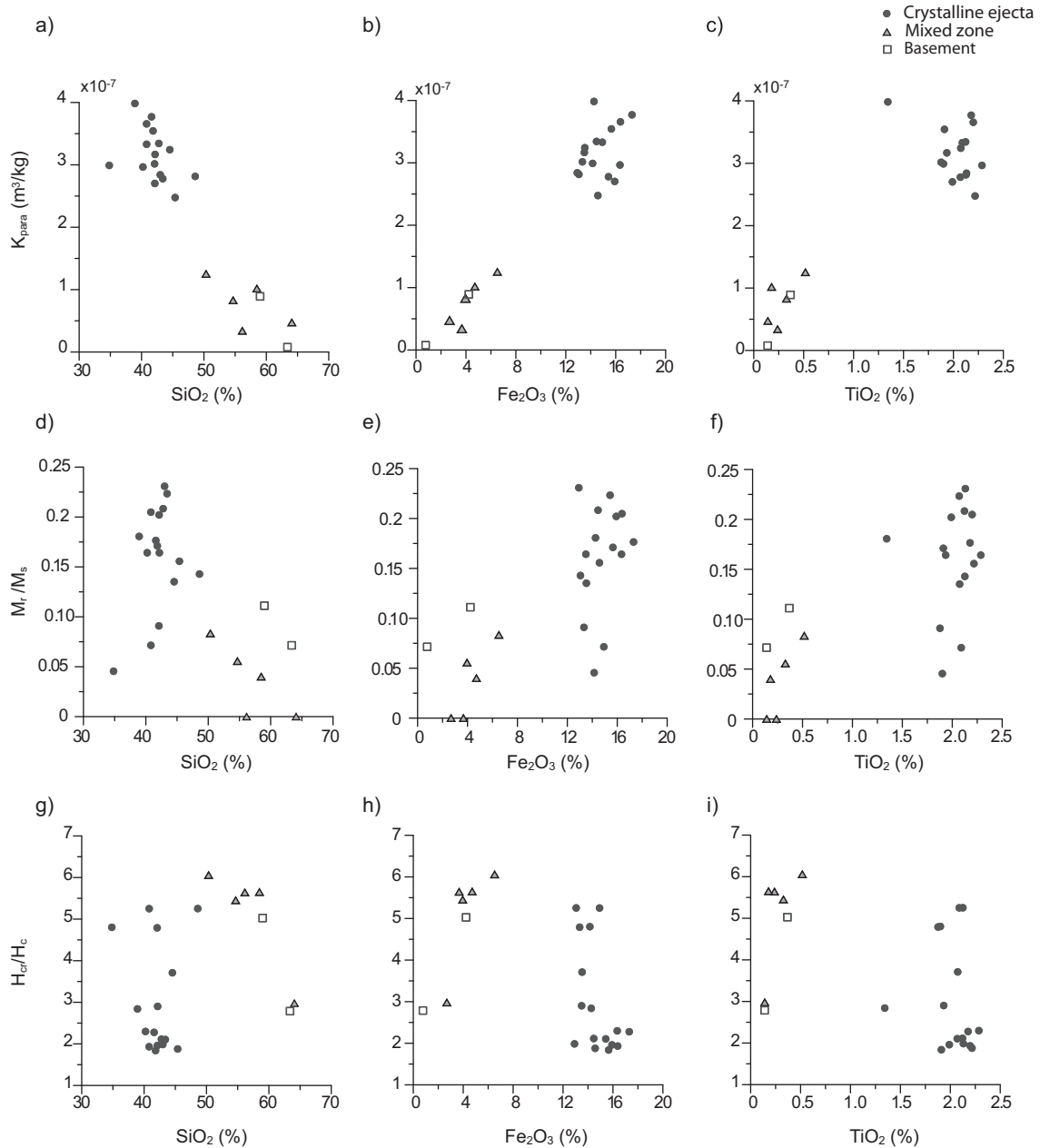


Fig. 12. Representation of the dependence of the most relevant major elements to different magnetic parameters. Paramagnetic susceptibility vs. (a) SiO₂, (b) Fe₂O₃, and (c) TiO₂ content; magnetization ratio M_r/M_s vs (d) SiO₂, (e) Fe₂O₃, and (f) TiO₂ content and coercivity ratio, H_{cr}/H_c vs (g) SiO₂, (h) Fe₂O₃, and (i) TiO₂ content.

(less than 300 °C at impact center) suggests that it could be the reason for this hardening. A core-shell structure of magnetite-maghemite is proposed as the magnetic structure responsible of this hardening.

Altogether, the data are in favor of the first possibility that the observed magnetic properties and the variations in grain size of the mafic rock (Fig. 2) are primary. This implies that, although severely brecciated, the mafic part of the ejecta at the location of Lockne-9 is a slab of rock that has been brecciated by the impact, but emplaced by the ejecta flow as a coherent body.

Based on the standard relation between ballistic ejecta at the crater rim and the distance from where it would have travelled within the crater (e.g., Melosh, 1989), we can estimate that the mafic ejecta would originate from somewhere near the pre-impact shear zone (dashed

line in Fig. 1) that has been suggested to pass the center of the crater (Högström et al., 2010).

This model has implications for our understanding how material, although suffering strong brecciation, may be emplaced and ejected without major blending during the cratering.

5. Conclusions

The visual core log shows the ejecta flap to be mainly a brecciated mafic rock, likely derived from an ejected dolerite, with some blending with sedimentary target rock (Cambrian alum shale) just at the contact between the ejecta and the more intact granitic basement.

Different lithologies can be distinguished by measuring their paramagnetic susceptibility.

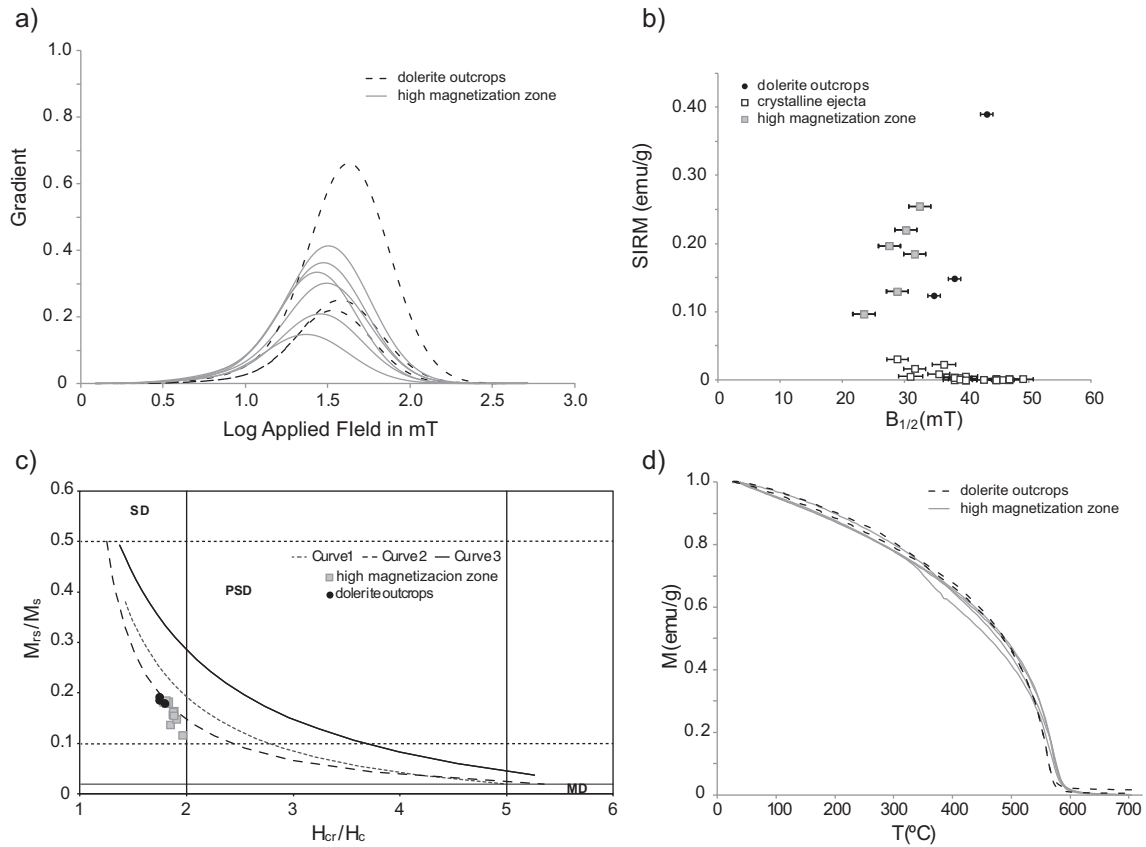


Fig. 13. Comparison between the high magnetization zone from the Lockne-9 core (between 11.40 and 12.50 m) and reference measurements from dolerite outcrops in the vicinity of Lockne crater. (a) Coercivity spectra of IRM curves where dashed lines represent measurements from the dolerite outcrops and solid lines represent measurements from the anomalous zone in the core. (b) Synthetic IRM versus $B_{1/2}$ of the main magnetic components, (c) Day plot, and (d) heating curve of the magnetization as function of temperature between 0 and 700 °C. Dashed lines represent samples from Lockne dolerite outcrops and solid lines represent measurements from the anomalous zone in Lockne-9 core.

The ferromagnetic susceptibility (initial and low-field bulk susceptibility) displays a maximum value in the crystalline ejecta that can be used in the stratigraphic description of the ejecta flap.

The ferromagnetic phases found in the Lockne-9 core are mainly magnetite/titanomagnetite, recognized by their thermomagnetic and IRM acquisition curves. They can potentially carry a stable remanent magnetization. Such studies will provide better constraints for future magnetic surveys of the Lockne crater.

The thermomagnetic curves combined with the coercivity spectra confirm that a distinct magnetic anomaly observed in the susceptibility and magnetization measurements is a primary feature already existing in the mafic rock before ejecta emplacement. A comparison with magnetic properties of dolerites unaffected by the impact indicates that this mafic rock most likely belongs to the suite of known dolerites

in the Lockne area. This emphasizes how rock magnetic properties may be helpful to determine if an ejecta body, even though severely brecciated, has moved as finite particles or *en masse*, information that is of paramount importance for the understanding of the cratering process.

Supplementary data to this article can be found online at <http://dx.doi.org/10.1016/j.jappgeo.2014.11.009>.

Acknowledgments

The work by I. Melero-Asensio and J. Ormó is partially supported by grants AYA2008-03467/ESP and AYA2011-24780-ESP. F. Martín-Hernández was partially funded by a Ramón y Cajal contract, all from the Spanish Ministry of Economy Competitiveness. The authors are grateful for the laboratory assistance by S. Guerrero-Suárez and

Table 2

Hysteresis parameters from samples of the unaffected dolerite outcrops and the high magnetization zone.

Sample	M_s (Am ² /kg)	M_r (Am ² /kg)	H_c (mT)	H_{cr} (mT)	K_{para} (m ³ /kg)	K_{int} (m ³ /kg)	M_r/M_s	H_{cr}/H_c
LOCDO14	0.90	0.16	17.04	30.61	9.05×10^{-5}	5.70×10^{-3}	0.18	1.80
2012LD1	0.75	0.14	16.25	28.34	9.27×10^{-5}	5.08×10^{-3}	0.19	1.74
12LOC2	2.18	0.42	20.05	35.03	1.78×10^{-4}	1.21×10^{-2}	0.19	1.75
L9_11.47	1.57	0.22	11.16	20.60	1.25×10^{-4}	1.17×10^{-2}	0.14	1.85
L9_11.90	0.85	0.1	9.01	17.66	2.08×10^{-4}	7.28×10^{-3}	0.12	1.96
L9_12.10	0.98	0.18	13.88	25.23	2.30×10^{-4}	7.79×10^{-3}	0.18	1.82
L9_12.13	1.56	0.25	12.06	22.54	1.77×10^{-4}	1.26×10^{-2}	0.16	1.87
L9_12.19	1.54	0.28	13.81	24.76	1.79×10^{-4}	1.19×10^{-2}	0.18	1.79
L9_12.20	1.25	0.21	12.75	23.97	1.92×10^{-4}	9.96×10^{-3}	0.16	1.88
L9_12.23	1.17	0.19	12.47	23.35	2.02×10^{-4}	9.36×10^{-3}	0.16	1.87
L9_12.36	1.1	0.16	11.50	21.89	2.05×10^{-4}	8.86×10^{-3}	0.15	1.90
L9_12.45	0.93	0.14	12.12	22.76	1.97×10^{-4}	7.52×10^{-3}	0.16	1.88

V. Villasante from the UCM and M. P. Martín-Redondo and M. T. Rodríguez-Sampedro from the CAB. We acknowledge Professor David T. King Jr. at the Auburn University (AL, USA) for his help with the linguistics. We appreciate the helpful comments by the reviewers that greatly improved the paper.

References

- Angerer, T., Greiling, R.O., 2012. Fabric evolution at basement–cover interfaces in a fold-and-thrust belt and implications for décollement tectonics (Autochthon, Lower Allochthon, central Scandinavian Caledonides). *Int. J. Earth Sci.* 101, 1763–1788.
- Butler, R.F., 1992. *Paleomagnetism: Magnetic Domains to Geologic Terranes*. Blackwell Scientific Publications.
- Day, R., Fuller, M., Schmidt, V., 1977. Hysteresis properties of titanomagnetites: grain-size and compositional dependence. *Phys. Earth Planet. Inter.* 13, 260–267.
- Dekkers, M., 1988. Magnetic behavior of natural goethite during thermal demagnetization. *Geophys. Res. Lett.* 15, 538–541.
- Dunlop, D.J., 2002a. Theory and application of the Day plot (Mrs/Ms versus Hcr/Hc) 1. Theoretical curves and tests using titanomagnetite data. *J. Geophys. Res. Solid Earth* 107 (EPM–4).
- Dunlop, D.J., 2002b. Theory and application of the Day plot (Mrs/Ms versus Hcr/Hc) 2. Application to data for rocks, sediments, and soils. *J. Geophys. Res. Solid Earth* 107 (EPM–5).
- Dunlop, D., Özdemir, O., 1997. *Rock Magnetism: Fundamentals and Frontiers*, Cambridge Studies in Magnetism. Cambridge University Press, Cambridge.
- Egli, R., 2004a. Characterization of individual rock magnetic components by analysis of remanence curves, 1. Unmixing natural sediments. *Stud. Geophys. Geod.* 48, 391–446.
- Egli, R., 2004b. Characterization of individual rock magnetic components by analysis of remanence curves: 2. Fundamental properties of coercivity distributions. *Phys. Chem. Earth ABC* 29, 851–867.
- Elbra, T., Kontny, A., Pesonen, L., 2009. Rock-magnetic properties of the ICDP-USGS Eyreville core, Chesapeake Bay impact structure, Virginia, USA. *ICDP-USGS Deep Drill. Proj. Chesap. Bay Impact Struct. Results Eyreville Core Holes*. *Geol. Soc. Am. Spec. Pap.* 458.
- Frisk, A.M., Ormö, J., 2007. Facies distribution of post-impact sediments in the Ordovician Lockne and Tvären impact craters: indications for unique impact-generated environments. *Meteorit. Planet. Sci.* 42, 1971–1984. <http://dx.doi.org/10.1111/j.1945-5100.2007.tb00554.x>.
- Gault, D.E., Sonett, C.P., 1982. Laboratory simulation of pelagic asteroidal impact: atmospheric injection, benthic topography, and. *Geol. Implic. Impacts Large Asteroids Comets Earth*. 190, 69.
- Henkel, H., Reimold, W.U., 2002. Magnetic model of the central uplift of the Vredefort impact structure, South Africa. *J. Appl. Geophys.* 51, 43–62. [http://dx.doi.org/10.1016/S0926-9851\(02\)00214-8](http://dx.doi.org/10.1016/S0926-9851(02)00214-8).
- Henkel, H., Reimold, W.U., Koeberl, C., 2002. Magnetic and gravity model of the Morokweng impact structure. *J. Appl. Geophys.* 49, 129–147.
- Heslop, D., Dekkers, M.J., Kruijer, P.P., Van Oorschot, I.H.M., 2002. Analysis of isothermal remanent magnetization acquisition curves using the expectation–maximization algorithm. *Geophys. J. Int.* 148, 58–64. <http://dx.doi.org/10.1046/j.0956-540x.2001.01558.x>.
- Heslop, D., McIntosh, G., Dekkers, M.J., 2004. Using time- and temperature-dependent Preisach models to investigate the limitations of modelling isothermal remanent magnetization acquisition curves with cumulative log Gaussian functions. *Geophys. J. Int.* 157, 55–63. <http://dx.doi.org/10.1111/j.1365-246X.2004.02155.x>.
- Högström, A.E., Sturkell, E., Ebbestad, J.O.R., Lindström, M., Ormö, J., 2010. Concentric impact structures in the Palaeozoic of Sweden—the Lockne and Siljan craters. *GFF* 132, 65–70.
- Jasonov, P., Nourgaliev, D., Burov, B., Heller, F., 1998. A modernized coercivity spectrometer. *Geol. Carpath.* 49, 224–226.
- Kontny, A., Elbra, T., Just, J., Pesonen, L.J., Schleicher, A.M., Zolk, J., 2007. Petrography and shock-related remagnetization of pyrrhotite in drill cores from the Bosumtwi Impact Crater Drilling Project, Ghana. *Meteorit. Planet. Sci.* 42, 811–827.
- Kruijer, P.P., Dekkers, M.J., Heslop, D., 2001. Quantification of magnetic coercivity components by the analysis of acquisition curves of isothermal remanent magnetisation. *Earth Planet. Sci. Lett.* 189, 269–276.
- Lindgren, P., Parnell, J., Norman, C., Mark, D.F., Baron, M., Ormö, J., Sturkell, E., Conliffe, J., Fraser, W., 2007. Formation of uranium–thorium-rich bitumen nodules in the Lockne impact structure, Sweden: a mechanism for carbon concentration at impact sites. *Meteorit. Planet. Sci.* 42, 1961–1969. <http://dx.doi.org/10.1111/j.1945-5100.2007.tb00553.x>.
- Lindström, M., Sturkell, E.F., 1992. Geology of the Early Palaeozoic Lockne impact structure, central Sweden. *Tectonophysics* 216, 169–185.
- Lindström, M., Sturkell, E.F.F., Törnberg, R., Ormö, J., 1996. The marine impact crater at Lockne, central Sweden. *GFF* 118, 193–206. <http://dx.doi.org/10.1080/11035899609546255>.
- Lindström, M., Ormö, J., Sturkell, E., Dalwigk, I., 2005a. The Lockne Crater: Revision and Reassessment of Structure and Impact Stratigraphy. In: Koeberl, C., Henkel, H. (Eds.), *Impact Tectonics, Impact Studies*. Springer, Berlin Heidelberg, pp. 357–388.
- Lindström, M., Shuvalov, V., Ivanov, B., 2005b. Lockne crater as a result of marine-target oblique impact. *Planet. Space Sci.* 53, 803–815.
- Louzada, K.L., Stewart, S.T., Weiss, B.P., Gattacceca, J., Bezaeva, N.S., 2010. Shock and static pressure demagnetization of pyrrhotite and implications for the Martian crust. *Earth Planet. Sci. Lett.* 290, 90–101.
- Lowrie, W., 1990. Identification of ferromagnetic minerals in a rock by coercivity and unblocking temperature properties. *Geophys. Res. Lett.* 17, 159–162.
- Melosh, H.J., 1989. *Impact cratering: a geologic process*, Oxford monographs on geology and geophysics. Oxford University Press.
- Moskowitz, B.M., 1981. Methods for estimating Curie temperatures of titanomagnemites from experimental J_s - T data. *Earth Planet. Sci. Lett.* 53, 84–88.
- Mullender, T., Velzen, A.J., Dekkers, M., 1993. Continuous drift correction and separate identification of ferrimagnetic and paramagnetic contributions in thermomagnetic runs. *Geophys. J. Int.* 114, 663–672.
- O'Reilly, W., 1976. Magnetic minerals in the crust of the Earth. *Rep. Prog. Phys.* 39, 857.
- Ormö, J., Lindström, M., 2000. When a cosmic impact strikes the sea bed. *Geol. Mag.* 137, 67–80 (doi:null).
- Ormö, J., Lindström, M., 2005. New Drill-Core Data from the Lockne Crater, Sweden: The Marine Excavation and Ejection Processes, and Post-Impact Environment. 36th Annual Lunar and Planetary Science Conference, p. 1124.
- Ormö, J., Gómez-Ortiz, D., Komatsu, G., Bayarara, T., Tserendug, S., 2010a. Geophysical survey of the proposed Tsenkher impact structure, Gobi Altai, Mongolia. *Meteorit. Planet. Sci.* 45, 373–382.
- Ormö, J., Hill, A.C., Self-Trail, J.M., 2010b. A chemostratigraphic method to determine the end of impact-related sedimentation at marine-target impact craters (Chesapeake Bay, Lockne, Tvären). *Meteorit. Planet. Sci.* 45, 1206–1224.
- Ormö, J., Rossi, A.P., Housen, K.R., 2013. A new method to determine the direction of impact: Asymmetry of concentric impact craters as observed in the field (Lockne), on Mars, in experiments, and simulations. *Meteoritics & Planetary Science* 48, 403–419. <http://dx.doi.org/10.1111/maps.12065>.
- Patchett, P.J., 1978. Rb/Sr ages of Precambrian dolerites and syenites in southern and central Sweden. *Sver. Geol. Unders. C* 747, 1–63.
- Rochette, P., 1987. Magnetic susceptibility of the rock matrix related to magnetic fabric studies. *J. Struct. Geol.* 9, 1015–1020.
- Scott, R.G., Pilkington, M., Tanczyk, E.L., 1997. Magnetic investigations of the West Hawk, Deep Bay and Clearwater impact structures, Canada. *Meteorit. Planet. Sci.* 32, 293–308. <http://dx.doi.org/10.1111/j.1945-5100.1997.tb01267.x>.
- Shuvalov, V., Trubetskaya, I., 2008. Numerical simulation of the LCROSS impact experiment. *Sol. Syst. Res.* 42, 1–7.
- Shuvalov, V., Ormö, J., Lindström, M., 2005. Hydrocode simulation of the lockne marine target impact event. In: Koeberl, C., Henkel, H. (Eds.), *Impact Tectonics, Impact Studies*. Springer, Berlin Heidelberg, pp. 405–422.
- Sturkell, E.F.F., 1998. The marine Lockne impact structure, Jämtland, Sweden: a review. *Geol. Rundsch.* 87, 253–267. <http://dx.doi.org/10.1007/s005310050208>.
- Sturkell, E., Lindström, M., 2004. The target peneplain of the Lockne impact. *Meteorit. Planet. Sci.* 39, 1721–1731.
- Sturkell, E.F., Ormö, J., 1997. Impact-related clastic injections in the marine Ordovician Lockne impact structure, Central Sweden. *Sedimentology* 44, 793–804.
- Sturkell, E.F., Ormö, J., 1998. Magnetometry of the marine, Ordovician Lockne impact structure, Jämtland, Sweden. *J. Appl. Geophys.* 38, 195–207.
- Sturkell, E.F., Broman, C., Forsberg, P., Torssander, P., 1998a. Impact-related hydrothermal activity in the Lockne impact structure, Jämtland, Sweden. *Eur. J. Mineral.* 10, 589–606.
- Sturkell, E.F.F., Ekelund, A., Törnberg, R., 1998b. Gravity modelling of Lockne, a marine impact structure in Jämtland, central Sweden. *Tectonophysics* 296, 421–435. [http://dx.doi.org/10.1016/S0040-1951\(98\)00149-8](http://dx.doi.org/10.1016/S0040-1951(98)00149-8).
- Sturkell, E., Ormö, J., Lepinette, A., 2013. Early modification stage (preresurgence) sediment mobilization in the Lockne concentric, marine-target crater, Sweden. *Meteorit. Planet. Sci.* 48, 321–338. <http://dx.doi.org/10.1111/maps.12058>.
- Törnberg, R., Sturkell, E.F.F., 2005. Density and magnetic susceptibility of rocks from the Lockne and Tvären marine impact structures. *Meteorit. Planet. Sci.* 40, 639–651. <http://dx.doi.org/10.1111/j.1945-5100.2005.tb00968.x>.
- Tudryn, A., Tucholka, P., 2004. Magnetic monitoring of thermal alteration for natural pyrite and greigite. *Acta Geophys. Pol.* 52, 509–520.